Journal of Basic and Environmental Sciences, 5 (2018) 245-251

ISSN

Online: 2356-6388

Print: 2536-9202

Research paper

Open Access

High Efficiency solar cell based on ZnO/Carbon Nanotube-Graphene Nanocomposite

Mohamed Mokhtar Mohamed [a*], S.M. Reda [a], M. Khairy [a,b], Eman M. Naguib[a]

[a]Benha University, Faculty of Science, Chemistry Dept., Benha, Egypt

[b]Chemistry Department, College of Science, Al-Imam Mohammad Ibn Saud lslamic University, Riyadh, KSA

***Corresponding author**; Mohamed Mokhtar Mohamed (e-mail: mohmok2000@yahoo.com).

Abstract

ZnO nanoparticles on carbon nanotube, graphene and carbon nanotube-graphene composites at a ratio of 1:1, were synthesized via a surfactant free approach. All samples were characterized by XRD, TEM and N_2-adsorption (BET technique). The electrical conductivity of samples was measured. The composites obtained were used in solar cell application. The characterization results show the strong interaction between G and CNT; via hydrogen bonding, that was then well maneuvered by dispersion of ZnO nanocrystallites (of an average diameter of 22 nm). The results show a greater surface area and pore radius values (227.5 m^2/g, 58.9Å) of the ZnO/Carbon nanotube-graphene composite compared to other composites. The assembled dye sensitized solar cell of the photoanode ZnO/Carbon nanotube-graphene shows the greatest performance with a power conversion efficiency comprised of 7.76%.

Keywords: DSSCs; ZnO/CNT-Graphene; ZnO/CNT; Electron transfer

Received; 3 May 2018, Revised form; 4 Jun 2018, Accepted; 10 Jun 2018, Available online 1 July 2018

1. Introduction

The 2D graphene restacking is one of the effects that impede its catalytic characteristics via reducing the available active sites and the restriction consequences correlated to the reactants diffusion between the layers. Moreover, enlarging the graphene basal plane hinders electron transfer and thus slowdown the reaction kinetics [1, 2]. To obviate such declines in graphene catalytic performances, a hybridization with CNT is functioned to work as a spacer for graphene nanosheets and to boost the electronic conductivity of the hybrid. The synergistic effects created by the 3D construction obtained via 2D graphene and 1D CNT have shown high activity toward ORRs performed in acidic media and when incorporated with Fe [3]. The overall electrical and mechanical characteristics can be improved by the hybrid systems [4] and demonstrated that Cu involvement exhibits high lucidity and electrical conductivity based on CNT-reinforcing graphene structure [5]. Some difficulty during fabrication of hybrid (CNT-graphene) appears such as weak bonding, created defects as well as conductivity declining throughout the remnant oxides on their surfaces, which created to facilitate their mutual interactions in the first place [6]. Accordingly, the combination of graphene/CNT composite could offer a potential answer during assembly in solar cells via accelerating electron transfer; through the adhered CNT and G interface, and affording high surface areas for dyes immobilization. However, the reported power conversion efficiency while using such composite has shown very naïve values (e.g. 0.85% [7]).

In order to enhance the photovoltaics characteristics of the hybrid, ZnO; as a translucent conducting oxide, was incorporated to enhance the optical properties [8, 9] and to construct a heterojunction at the CNT/graphene interface to control the electron-hole recombination processes [10, 11]. The cheap ZnO modified CNT/graphene composite is going to prevent graphene restacking and managing the bundle shrinkage of CNTs; used to affect its activity during solution reforming processes [12], beside the electrical conductivity and optical properties ZnO can add to the composite. An expected Schottky barrier between ZnO (n-type) and the residual oxides localized on CNT-graphene (p-type) is presumed to regulate the recombination of the photo-excited electron–hole pairs [13]. In this work, the ZnO incorporated CNT-graphene composite was prepared by means of a facile sonication-hydrothermal-calcination approach with the use of commercially available zinc nitrate, graphene oxide and oxygen functionalized multi-walled carbon nanotubes as precursors. These composite materials were tested as anodes in solar cell application via using the dye-sensitized approach (DSSC). Successfully, the DSSC based on reduced graphene functionalized CNT films produced conversion efficacy of 5.29% exceeding that of

graphene oxide/CNT films [14]. The fabricated CNTs/polythiophene hybrid generated conversion efficiency of 4.72%, which approached the vertically aligned single-walled carbon nanotubes [15], that gives a conversion efficiency of 5.5% [16]. The as-synthesized sponge-like CNTs that owned homogeneous nanoscale structure with great porosity shows a conversion efficiency of 6.21% [17]. These aforementioned catalysts necessitate hard conditions during fabrication and they are rather costly. Thus, designing a photoanode with an efficient charge transport to the current collector is going to improve the DSSC performance. This indeed is going to be achieved via modulating the surface texturing of the incorporated hybrid, band gap decrement, increasing active sites and charge transfer improvement with minimizing their recombination at the formed interface. Assembling the ZnO/CNT-G heterojunction cell of superior flexibility achieved a moderately high PCE up to 7.7 %. The aim of this work is how to create devices of high solar energy collection capacity via employing cheaply viable nanomaterials with scalable and simple production techniques. The composite materials are characterized by X-ray diffraction (XRD), transmission electron microscopy (TEM), electronic conductivity and N_2 adsorption.

2. Preparation methods

2.1. Preparation of GO

Graphene oxide (GO) was prepared from natural graphite according to a modification of the Hummers–Offeman method.

2.2. Preparation of ZnO NPs

Three grams of urea and one gram of zinc acetate were dissolved in 50 mL de-ionized water containing polyethylene glycol (0.5 g/50 ml, M.wt=4000), and stirred for 35 min. Then, this transparent solution was transferred to an oven heated at 100 ºC for 5 h. The obtained precipitate was then centrifuged, washed, and dried at 65 ºC. Finally, the ZnO nanoparticles were obtained after annealing at 300◦C for 4 h in an air atmosphere.

2.3. Preparation of ZnO incorporated CNT-graphene

The as-synthesized ZnO (0.5 gm) dissolved in 100 ml mixture of ethanol-water (1:1) was stirred for 1 h and then poured onto the mixture of CNT-graphene formed at 1:1weight % ratio i.e. the weight ratio percentage concentration of ZnO is 50%**.** This mixture was sonicated for 2 h and then autoclaved at 150ºC for 18 h followed by the same procedure mention for the hybrid fabrication. The individual analogue ZnO/CNT and ZnO/graphene was also synthesized in a typical procedure and the ratio of ZnO to either CNT or graphene was to give a weight % ratio of 50%.

2.4. Photovoltaic efficiency measurements

The viscous paste of ZnO/CNT-graphene, ZnO-CNT and ZnO-graphene samples formed with 1.0 ml triton X-100 was delivered onto FTO-conducting glass of a resistance equal 18 Ω cm^{-1}. The films were fired at 300ºC for 1 h and then engrossed in the N719 dye of concentration of 2.7 x 10^{-4} mol L^{-1} for 36 h at room temperature. The counter electrode that consisted of the same conducting glass and coated with a very thin graphite film was placed directly on the top of the dye coated the composite films, permitting the two ends of the glass for application of electrical contact. The electrolyte containing 0.03M I_2-0.3 M KI dissolved in acetonitrile was injected via the capillary force into the inter electrodes space. The I–V characteristic for the cell was measured in the presence of light using AM 1.5 G lamp at a light intensity of 100 mw/cm^2. The voltage and current were recorded using Keithly voltammeter 175A and Keithly electrometer 614, respectively. The fill factor was calculated using the following relation: $FF = V_m I_m/V_{OC} I_{SC,}$ where V_m and I_m are respectively, voltage and current for maximum power output. The solar cell efficiency is calculated (η_y) using the following relation: $\eta_y = V_{oc} I_{sc} FF/ P_{in}$ where P_{in} is the power of the incident light.

2.5. Characterization Techniques

X-ray diffractions (XRD) are measured at room temperature using a Philips diffractometer (type Pw-3710); equipped with Ni-filtered copper radiation (λ = 1.5404Å), at 30 kV and 10 mA with a scanning speed of 2θ = 2.5º/min. The surface properties specifically BET surface area, total pore volume (V_p) and mean pore radius (r) are determined from N_2 adsorption isotherms measured at 77 K using Digisorp technique and the samples are out-gassed at 473 K for 3 h at a pressure of 10^{-5} Torr, before starting the measurement. TEM micrographs are measured using a FEI; model Tecnai G20, Super twin, double tilt 1010, at an accelerating voltage of 200 KV.

3. Results and discussion

3.1. XRD and TEM investigation

The XRD results of ZnO-CNT, ZnO-G and ZnO incorporated CNT-graphene (Zn/CNT-G) are presented in Fig (1) The ZnO-CNT pattern shows a hexagonal wurtzite structure (JCPDS Data Card No: 36-1451) of well resolved diffraction peaks indexed to (1 0 0), (0 0 2), (1 0 1), (1 0 2), (1 1 0), (1 0 3), (2 0 0), (1 1 2) and (2 0 1) planes with higher intensities compared to that in ZnO-G, where it suffers a marked decrease in ZnO/CNT-G. The ZnO/CNT-G pattern displays a peak at 2θ=25.45º due to the (002) plane of carbon, which disappeared in ZnO-G and objectively detected in ZnO/CNT. Increasing the ZnO peaks intensities in the ZnO-CNT pattern may propose a decrease in the interaction between CNT and the ZnO crystals.

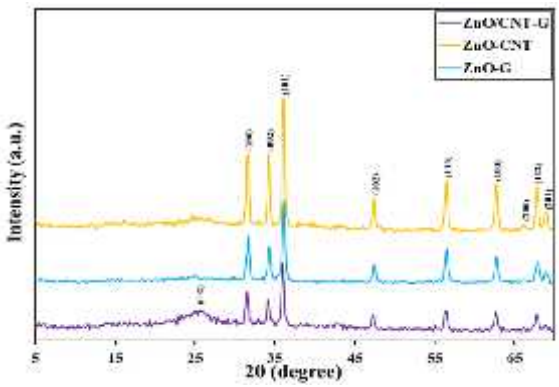

Fig (1): XRD patterns of ZnO/CNT-G, ZnO/CNT and ZnO/G catalysts.

The existence of the crystal plane (002); due to reduced carbonaceous moieties, in ZnO-CNT while its fading in ZnO-G and remerging in Zn/CNT-G with higher broadness than the former could give a hint about graphene restacking via dispersion of ZnO crystallites. This also estimates not only the stimulating ability of CNT towards graphene reduction but also the strong interaction between CNT and graphene sheets in addition to ZnO crystallites. Consistently, the crystallites size determined by Scherrer equation estimates a value of 42 nm for ZnO-CNT and 33 nm for ZnO-G; as determined from the intense (101) plane of ZnO, and diminishes into 29 nm in Zn/CNT-G. Interestingly, the latter sample suffers a decrease in d-spacings comparatively probably due to strain (crystal faults) and surface roughness effects, emphasized via the broadness discussed before.

Fig (2) shows the morphologies of the ZnO-CNT, ZnO-G and ZnO/CNT-G nanocomposites. The TEM image of ZnO-CNT, shows big spherical particles of ZnO of an average diameter of 60 nm, comprehending the facile crystallization of ZnO on CNTs and to the strong interaction between them, evident from the morphology change. The SAED pattern (inset) indicates that ZnO decorates CNT via emergence of (100), (002), (101), (102) crystal facets of the former on (002) of the latter. Retaining the ZnO hexagonal array with an average diameter of 25 nm was remarkably seen on the graphene substrate (ZnO-G) with high capacity of agglomeration, and with a typical SAED pattern to that depicted for ZnO-CNT. Preserving the ZnO morphology could give a hint that the interaction with G is not strong as such. The TEM image of ZnO/CNT-G evidences the dispersion of ZnO into CNT and graphene as well as it exhibits the binding of CNTs; via its extended spider trap, with the graphene nanosheets. The latter combination between CNT and graphene affected the particle diameter of ZnO to be the lowest (22 nm) among all the samples and the morphology was typical to that existed for ZnO-CNT (mainly spherical), explaining the influential effect of CNT rather than graphene on the ZnO morphology.

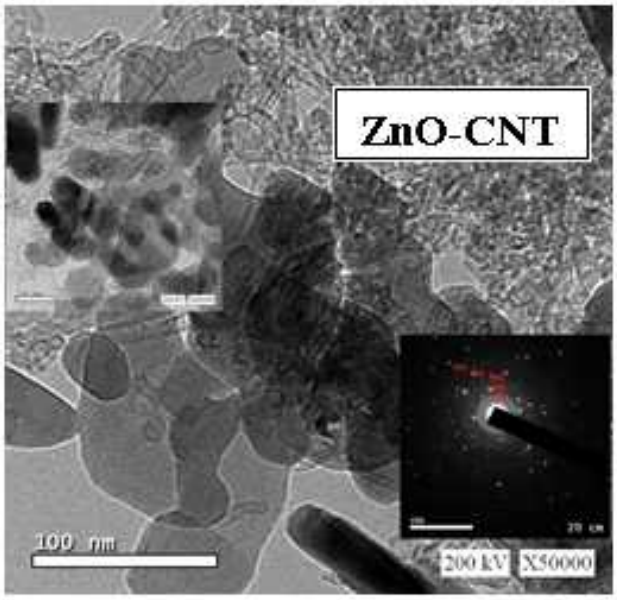

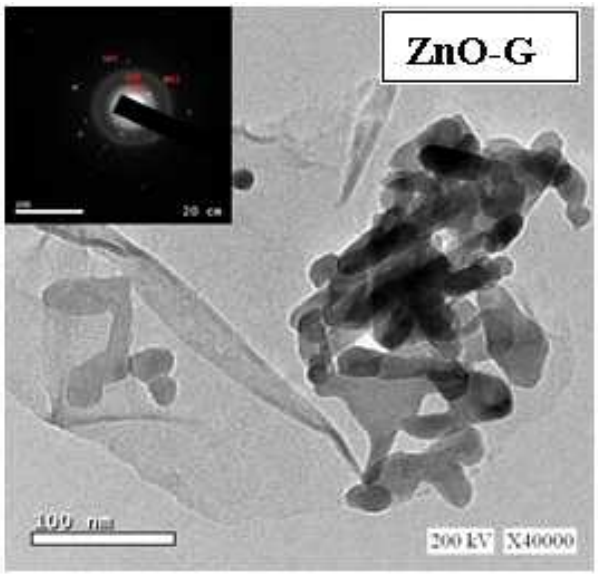

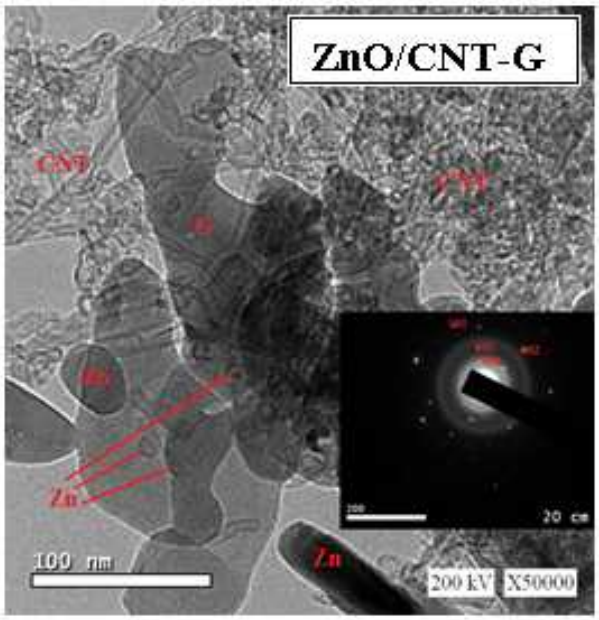

Fig (2): TEM and SAED (as inset) images of ZnO/CNT, ZnO/G and ZnO/CNT-G.

3.2. Surface properties

The surface texturing properties of the as-synthesized hybrids depicted via nitrogen adsorption-desorption isotherm are presented in Table (1). The catalysts isotherms (not shown); for the descriptive ones (ZnO-CNT and ZnO/CNT-G), show type IV characterized by hysteresis and steep rise at high relative pressures to confirm the mesoporosity existence.

Table (1): Surface texturing properties of ZnO-CNT and ZnO/CNT-G catalysts.

Sample	S_{BET} (m^2/g)	Pore radius $\bar{r}$ (Å)	Total Pore volume
ZnO-CNT	198.4	27.9	0.35
ZnO/CNT-G	227.5	58.9	0.34

The specific surface area of the ZnO/CNT-G composite together with pore radius and volume values were respectively, 227.5 m^2 g^{-1}, 58.9 Å and 0.34 cm^3g^{-1}. These

values exceeded those depicted for ZnO/CNT (198.4 $m^2 g^{-1}$ and 27.9 Å) while keeping that of the pore volume unchanged (0.34 $cm^3 g^{-1}$). This clarifies the involvement of graphene within CNT spider array as established via increasing the S_{BET} by 1.15 times that of ZnO/CNT as well as increasing the pore radius values by 2 times that of the latter.

3.3. Electronic conductivity of the nano-composites

The electron transfer ability of the as-synthesized nanocomposites was tested and presented in Fig (3). Apparently, CNT contained ZnO shows an excellent electron conduction whereas graphene containing ones illustrates higher resistivity. This result is consistent with an earlier report on graphene, which states that the low electron conductivity in graphene is due to its extremely low out-of-plane conductivity [18] as well as the low electron density on its basal plane [19].

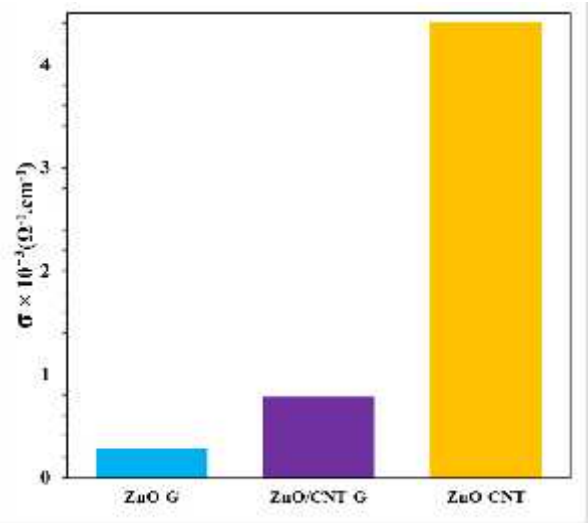

Fig (3): Conductivity result of ZnO/CNT-G, ZnO/CNT, ZnO/G and CNT-G.

In this context, the sequence of decreasing the conductivity was in the order; ZnO/CNT (4.6×10^{-3} $\Omega^{-1}cm^{-1}$) > ZnO/CNT-G (0.8×10^{-3} $\Omega^{-1}cm^{-1}$) > ZnO-G (0.23×10^{-3} $\Omega^{-1}cm^{-1}$). Illustratively, the graphene resistivity is successfully decreased via decoration with CNTs (ZnO/CNT-G) but still lower than ZnO/CNT, wherein CNT acts as a tunnel for facilitating electron transfer. It seems that increasing the crystallinity of ZnO grown on CNT rather than on graphene; as XRD and TEM confirmed, assists electrons transfer through well-defined channels. The involvement of graphene within the ZnO/CNT array; as N_2 sorptiometry confirmed, could induce interfacial resistance that decreases the conductivity when graphene/CNT composite is formed. Also, stacking graphene layers in the ZnO/CNT-G catalyst by ZnO; as XRD and TEM emphasized, could help the leakage of phonons across the interface and rather enhance its scattering. This outcome was supported by the results obtained when graphene sheets are stacked into paper sheets, and intercalated by CNT [20-21]. Although oxides functionalization on either CNT or G are very important for binding them together, however, their prominent existence together with moistures; especially on G surfaces, affect much the electron transfer process as it works as p-type semiconductor capable of grasping electrons.

3.4. Photovoltaic performance of nano-composite photoanodes-modified DSSCs

The photovoltaic performances of ZnO-CNT, ZnO-G, ZnO/CNT-G photoanode-customized DSSCs under mimicked solar irradiation of AM 1.5 G were investigated by analyzing the J-V profiles, which are shown in Fig (4). The resultant photovoltaic factors are reordered in Table (2). A marked boost in the short-circuit current up to 176 mA/cm^2 is depicted in the J-V curve of ZnO/CNT-G compared to all DSSCs based on ZnO (2.15 mA/cm^2) to be in the sequence; ZnO-CNT (65 mA/cm^2) > ZnO-G (3.9 mA/cm^2). The ZnO/CNT-G-based DSSC displayed a conversion efficiency (η = 7.76%) that was 1.39% and 1.94%, higher than those of the DSSCs based on ZnO-CNT (η = 5.58%) and ZnO-G (η = 4.0%), respectively. However, the nanocomposites suffered from low open circuit potential (V_{OC}) perhaps due to recombination losses at the nano-linkage zone [22-23].

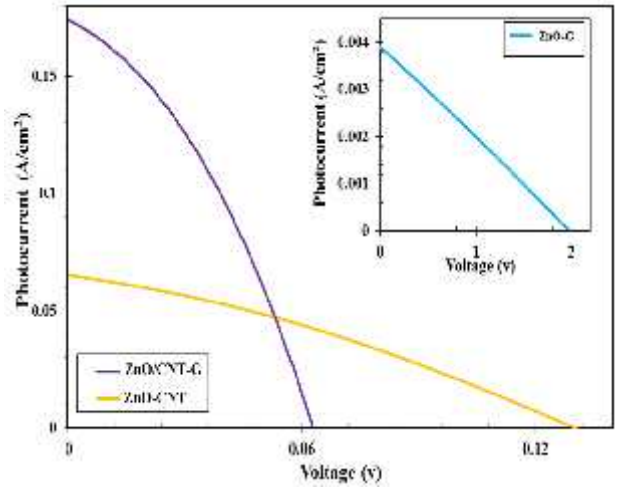

Fig (4): J−V curves of typical DSSC Cells of ZnO/CNT-G and ZnO/CNT under 1 sun illumination. The inset shows ZnO/G cells.

The V_{OC} of ZnO/CNT-G was 0.063 V where it was 2.0 V for ZnO-G and 0.13 V for ZnO-CNT, in which ZnO exhibited the highest crystallinity. This result stresses that the ZnO crystallinity is not the only factor to be responsible for the electron transport via specified channels since ZnO-G; of higher Voc, indicates lower electronic conductivity than both ZnO-CNT and ZnO/CNT-G (Fig (3)) cells. Excitingly, the ZnO-G cell that generated the highest Voc exhibited lower efficiency (η = 4.0%) than that achieved by ZnO/CNT-G (η = 7.76%), which offered the highest J_{SC} factor. This indeed amplifies the efficiency dependence on the high surface area, large pore radius and small crystallites size of the ZnO incorporated CNT-G cell; as emphasized from N_2 adsorption and TEM results, which seriously affected the dye adsorption and amplify the amount of adsorbed light.

Table (2): Photovoltaic parameters of the fabricated DSSCs. The performance was assessed using 100 mw cm^{-2} simulated AM 1.5G solar light irradiation. J_{sc}; Short-circuit current density; V_{oc}; Open-circuit voltage; J_m: Maximum photocurrent density; V_m; Maximum photovoltage; FF; Fill factor; η; Power conversion efficiency.

sample	I_{sc}(mA)	V_{oc}(V)	lm(mA)	V_m(V)	ff	η%
ZnO-CNT	65	0.13	44	0.062	0.33	5.58
ZnO-G	3.9	2	2.4	0.83	0.26	4
ZnO/CNT-G	176	0.063	120	0.032	0.35	7.76

Additionally, the high recombination potential on the ZnO-G cell; although it exceeds ZnO-CNT, nullifies the dependence of its Voc value only on the interface between ZnO and G. However, the limited light collected and the low electron transport pathway of ZnO/G; electronic conductivity confirmed, illustrates that the proper anchoring of ZnO on graphene sheets rather than that of ZnO on CNT could be the one responsible for increasing the Voc of the former (ZnO-G). Decreasing the electron mobility of ZnO-G as electronic conductivity confirms eliminates the electronic leakage (i.e. electron transfer from ZnO to triiodide to generate iodide is almost excluded) and rather organizes its transfer via the established interface points (facets) causing an increase in the Voc value. Increasing the crystallites size of ZnO in ZnO-CNT cell; as XRD and TEM indicated, might lead to formation of grain boundaries that prolong the diffusion time transmitted by electrons and thus affect the efficiency. Contrarily, decreasing the ZnO crystallite size on G support decreases the ZnO-ZnO contacts and with graphene to reduce recombination consequences and to improve the device efficiency. However, offering lower conversion efficiency compared to ZnO/CNT-G is mainly due to the limited light absorption, decreased surface area and the consequences mentioned thereof. Since ZnO facets are almost similar as depicted from SAED profiles when deposited on different carbon substrates; i.e. similar junction facet area, the imperfection prone on CNT, G and CNT-G are the prime factors to affect the Voc and Isc parameters. Accordingly, the exhibited defects on CNT-G and following ZnO incorporation are seriously affected the Voc parameter although this cell possessed high conductivity value. This emphasizes the importance of the catalyst surface defects on controlling the electron leakage as well as managing the recombination process to boost the photovoltaic efficiency. The J_{max} and V_{max} parameters of all devices followed trends close to those of Jsc and Voc (Table 2).

3.5. Electrochemical behavior of the nanocomposites

The electrochemistry descriptions for all nanocomposites are measured at 25ºC. To examine the catalytic properties of all nanocomposites, CV is employed to evaluate their response toward I_3^- reduction; to mimic that occurring during DSSC performance, via using both peak current (E_P) and peak to peak separation (E_{pp}) values. Enhancing the former and decreasing the latter values point to higher electro-catalytic activity [24]. Fig (5) shows the cyclic voltammograms of ZnO-CNT, ZnO-G and ZnO/CNT-G nanocomposites. Each compound displays one anodic and one cathodic current peaks of slightly varied position. Such couple of redox peaks was perceived in all nanocomposite curves, indicating direct electron transfer between I_3^- and ZnO containing different carbon substrates. The ZnO/CNT-G nanocomposite show anodic peak current density at 0.038 A g^{-1} and cathodic peak current density at -0.26 A g^{-1}; that responsible for the I_3^- reduction into I^- in DSSCs [25, 26]. Whereas, those of the ZnO-G electrode indicate anodic current at 0.037 A g^{-1} and cathodic current at -0.31 A g^{-1} exceeding those of the ZnO-CNT electrode (anodic current at 0.04 A g^{-1} and cathodic current at -0.24A g^{-1}).

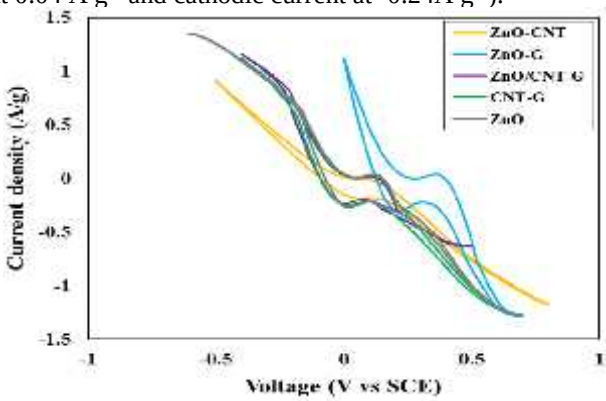

Fig (5): Cyclic voltammetry studies of I_3^- reduction at the electrodes of ZnO/CNT, ZnO/G and ZnO/CNT-G at 10 mV/s scan rate.

Indeed, higher current densities are likely due to increasing the active surface area of the mesoporous composites, which responsible for speeding up the redox reaction. However, shifting the cathodic potential into more negative values as in ZnO/CNT-G (-0.01 V) together with enhancing its current density facilitates the reduction of $I_3^-$and rather confirms the strong adsorption of iodide ions onto the nanocomposite surfaces (ZnO/CNT-G). The redox behavior in triiodide/iodide electrolyte is principally follows the subsequent reactions:

$3I^- \rightarrow I_3^- + 3e$ (at negative potential)

$2I_3^- \rightarrow 3I_2 + 2e$ (at positive potential)

The E_{pp} values calculated based on the differences between E_p (anodic) and E_p (cathodic) were 0.35, 0.30 and 0.28 V for ZnO-G, (ZnO/CNT-G), and ZnO-CNT, respectively. This emphasizes that ZnO/CNT-G and ZnO-CNT nanocomposites can excellently used as potential photoanodes in DSSCs. The CV curves shape examined at high scan rates (100 mVs^{-1}) were comparable to those at low scan rates (5 mV s^{-1}; not shown) without evident alteration, referring to the efficient exceeding of both ionic and electronic transport rate inside the composite electrodes. In addition, the CVs indicate the presence of quasi–capacitance current with extended potential window in case of the composite ZnO/CNT-G, which is a good indication on the stability and strong interaction of ZnO

nanocrystallites within the CNT/G than in ZnO/CNT and ZnO/G.

The electronic properties, charge carrier densities and flat-band potentials (E_{FB}) of the formed nanocomposites were investigated by the Mott–Schottky (MS) plots [$\frac{1}{C^2} = \frac{2}{\varepsilon\varepsilon_0 e A^2 N_d}\left(V - V_f - \frac{k_B T}{e}\right)$]. As shown in Fig (6), the positive slopes of the M-S plots seen for all nanocomposite samples are diagnostic to the n-type semiconductors. The E_{FB} of the samples are -0.05 V, 0.0 V, 0.075 V for ZnO/CNT-G, ZnO/G and ZnO/CNT. Thus, the values determined for the CB are -0.25, -0.2 and -0.125 for the catalyst mentioned sequence ($C_B \approx E_{FB}$ -0.2 V) [27]. On the other hand, the ZnO/CNT-G electrode showed the highest positive V_B potential as compared to the others, testifying the highest donor density between all samples. Thus, the formation of p-n heterojunction at the ZnO (n-type)/CNT-G (p-type) interface is found to be responsible for enhancement of the redox performance of the I_3^-/I^- electrolyte. In conformity, the donor density determined via straight line sloping of ZnO/CNT-G (0.48 x 10^{20} cm^3) was rather larger than ZnO/graphene (0.25 x 10^{20} cm^3) and ZnO/CNT (0.12 x 10^{20} cm^3), manifesting the p-n interface formation and its role in achieving promising results in electro-optical devices as solar cells.

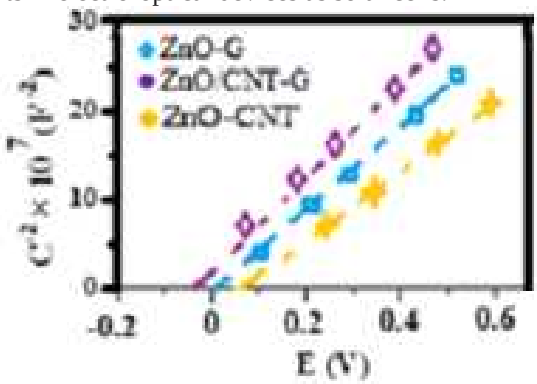

Fig (6): Mott–Schottky plots of ZnO/CNT, ZnO/G, ZnO/CNT-G and CNT-G catalysts.

The ZnO/CNT that exhibited the highest electronic conductivity presented lower charges density assigning that cations and anions other than electrons constitute high fraction of this composite conductivity per unit surface area.

Accordingly, the fabricated ZnO/CNT-G solar cell device is worked via injecting electrons from LUMO of the dye into the conduction band of ZnO to reach the surface of CNT-G composite structure. Increasing the PCE of ZnO/CNT-G is also due to varying the work function of the components forming the latter electrode, the work function of G is 4.4 eV whereas that of CNT is 4.8 eV. The work function of the hexagonal ZnO is about 5.076 eV [28] and it owns a conduction band around -4.2 eV and a band gap of 3.1 eV. The conduction band of ZnO possesses lesser value than work functions of graphene and CNT, such that charge transfer from the former to both of the latter is dynamically constructive.

Conclusively, the excited electrons from the dye N719 following illumination are expected to be injected into the conduction band of the ZnO nanocrystals and subsequently the dye^+ became oxidized, via receiving electrons from the electrolyte to be regenerated. Indeed, the latter (electrolyte) is likely regenerated thru the Pt counter electrode. The deposition of ZnO on the composite of CNT-G is very valuable since they act as an electron sink for efficient regulation of charges transfer beside their high absorbability toward dye molecules, assisting eventually in trapping light. This composite resulted in photocurrent boost and via the obtained minimization of charges recombination an improved in the DSSC performance is obtained.

4. Conclusions

The Schottky junction formed between n-type ZnO and P-type CNT/G in the composite consisting of ZnO/CNT-G affected the facile electron transfer via efficient electron hole separation to boost the PCE into 7.76%. Besides, it shows higher visible light absorptivity, greater transient photocurrent density and two fold increase in the pore radius as compared to the individual analogue ZnO/CNT and ZnO/G. Although ZnO/CNT-G exhibited some defects, it shows a moderately high electronic conductivity; indeed lower than ZnO/CNT, however, these defects did not impede the electron transfer as well as its lifetime. More correlations between specific capacities of nanocomposites, electronic conductivity, I_3^- diffusion distances and their influences on the photovoltaics were studied and well discussed.

References

[1] D.A.C. Brownson, L.j. Munro, D.K. Kampouris, C.E. Banks, RSC Adv. 1 (2011)978–988.

[2] J. Yan, T. wei, B. Shao, F.Q. Ma, Z.J. Fan, M.L. Zhang, C. Zheng, Y.C. Shang, w.Z.Qian, F. wei, Carbon 48 (2010) 1731–1737.

[3] S. Zhang, H. Zhang, Q. Liu, S. Chen, J. Mater. Chem. A 1 (2013) 3302–3308.

[4] M.S. Saha, A. Kundu, J. Power Sources 195 (2010) 6255-6261.

[5] E.E. Tkalya, M. Ghislandi, G. de with, C.E. Koning, Curr. Opin. Colloid 17 (2012) 225-231.

[6] F. Mirri, A.w.K. Ma, T.T. Hsu, N. Behabtu, S.L. Eichmann, C.C. Young, D.E. Tsentalovich, M. Pasquali, ACS Nano 6 (2012) 9737-9744.

[7] B. Smith, K. wepasnick, K.E. Schrote, H.H. Cho, w.P. Ball, D.H. Fairbrother, Langmuir 25 (2009) 9767-9776.

[8] S. T. Kochuveedu, Y. H. Jang, Y. J. Jang, D. H. Kim, Visible Light Active Photocatalysis on Block Copolymer Induced Strings of ZnO Nanoparticles Doped with Carbon, J. Mater. Chem. A 1 (2013) 898−905.

[9] J. Matos, A. García, L. Zhao, M. M. Titirici, Solvothermal Carbon-Doped TiO2 Photocatalyst for the Enhanced Methylene Blue Degradation under Visible Light, Appl. Catal. A 390 (2010) 175−182.
[10] Y. P. Zhu, T. Y. Ma, T. Z. Ren, J. Li, G. H. Du, Z. Y. Yuan, Highly Dispersed Photoactive Zinc Oxide Nanoparticles on Mesoporous Phosphonated Titania Hybrid. Appl. Catal. B 156−157 (2014) 44−52.
[11] H. C. Qin, w. Y. Li, Y. J. Xia, T. He, Photocatalytic Activity of Heterostructures Based on ZnO and N-Doped ZnO. ACS Appl. Mater. Interfaces 3 (2011) 3152−3156.
[12] A. Kay, M. Grätzel, Sol. Energy Mater. Sol. Cells 44 (1996) 99-117.
[13] L. Sang, Y. Zhao, C. Burda, Chem. Rev. 114 (2014) 9283–9318.
[14] Y. Tang, J.H. Gou, Mater. Lett. 64 (2010) 2513-2516.
[15] J. Luo, H.J. Niu, w.J. wu, C. wang, X.D. Bai, w. wang, Solid State Sci. 14 (2012) 145-149.
[16] P. Dong, C.L. Pint, M. Hainey, F. Mirri, Y. Zhan, J. Zhang, M. Pasquali, R.H. Hauge, R. Verduzco, M. Jiang, ACS Appl. Mater. Interfaces 3 (2011) 3157-3161.
[17] J. Chen, F. Meng, X. Gui, H. Sun, Z. Zeng, Z. Li, Y. Zhou and Z. Tang, Carbon 50 (2012) 5624–5627.
[18] F. Du, D.S. Yu, L.M. Dai, S. Ganguli, V. Varshney, A.K. Roy, Chem. Mater. 23 (2011) 4810-4816.
[19] D.A.C. Brownson, L.J. Munro, D.K. Kampouris, C.E. Banks, Rsc Adv. 1 (2011) 978-988.
[20] P. T. Araujo, M. Terrones, M.S. Dresselhaus, Defects and impurities in graphene-like materials, Materials Today 15(3) (2012) 98–109.
[21] W. Chen, L. Yan, Preparation of graphene by a low-temperature thermal reduction at atmosphere pressure, Nanoscale 2(4) (2010) 559-63.
[22] K. P. Musselman, A. Marin, L. Schmidt-Mende, J. L MacManus-Driscoll, Incompatible Length Scales in Nanostructured Cu2O Solar Cells, Adv. Funct. Mater 22 (2012) 2202−2208.
[23] Yuhas, B. D.; Yang, P. Nanowire-Based All-Oxide Solar Cells. J. Am. Chem. Soc. 131 (2009) 3756−3761.
[24] A.J. Bard, L.R. Faulkner, J. Leddy, C.G. Zoski, Electrochemical Methods: Fundamentals and Applications, wiley, New York, 2 (1980).
[25] F. Gong, X. Xu, G. Zhou, Z.-S. wang, Enhanced charge transportation in a polypyrrole counter electrode via incorporation of reduced graphene oxide sheets for dye -sensitized solar cells, Phys. Chem. Chem. Phys. 15 (2013) 546.
[26] w. Sun, T. Peng, Y. Liu, S. Xu, J. Yuan, S. Guo, X.-Z. Zhao, Hierarchically porous hybrids of polyaniline nanoparticles anchored on reduced graphene oxide sheets as counter electrodes for dye-sensitized solar cells, J. Mater. Chem. A 1 (2013) 2762.
[27] T. Cai, Y. Liu, L. wang, S. Zhang, Y. Zeng, J. Yuan, J. Ma, w. Dong, C. Liu, S. Luo, Applied Catalysis B: Environmental 208**,** 1 (2017).
[28] H. G. Agrell, J. Lindgren , A. Hagfeldt, Sol. Energy 75 (2003) 169.